

# Kolmogorov flow: Linear Stability and Energy Transfers in a minimal low-dimensional model

Soumyadeep Chatterjee<sup>1, a)</sup> and Mahendra K. Verma<sup>1, b)</sup>

*Department of Physics, Indian Institute Of Technology Kanpur, Kanpur 208016, India*

(Dated: 14 July 2020)

In this paper, we derive a four-mode model for the Kolmogorov flow by employing Galerkin truncation and Craya-Herring basis for the decomposition of velocity field. After this, we perform a bifurcation analysis of the model. Though our low-dimensional model has fewer modes than the past models, it captures the essential features of the primary bifurcation of the Kolmogorov flow. For example, it reproduces the critical Reynolds number for the supercritical pitchfork bifurcation and the flow structures of the past works. We also demonstrate energy transfers from intermediate scales to large scales. We perform direct numerical simulations of the Kolmogorov flow and show that our model predictions match with the numerical simulations very well.

Keywords: Kolmogorov flow, low-dimensional model, linear stability, bifurcation analysis.

**In the late 1950s, Kolmogorov urged the fluid community to explore the stability criteria of a shear flow with spatially-periodic forcing; a system referred to as the Kolmogorov flow. Since then, many researchers have attempted to address the above problem using analytical, numerical, and experimental tools. The leading analytical results involve infinite or a large number of interacting Fourier modes. The numerical calculations and low-dimensional models too involve many Fourier modes. In this paper, we construct a four-mode low-dimensional model using Galerkin truncation and Craya-Herring basis. Our minimal model of the Kolmogorov flow captures the essential features of its primary bifurcation and the critical Reynolds number very well. The model predictions are borne out in numerical simulations.**

## I. INTRODUCTION

Flow instability and transition to turbulence are important problems of fluid dynamics. Kolmogorov abstracted a simple shear flow with spatially-periodic forcing<sup>1-3</sup>, whose instability and bifurcation has been studied intensely over the years. Also, the Kolmogorov flow has been experimentally realized in several setups, including a soap film<sup>4</sup> and an electrolytic fluid<sup>5,6</sup>. In this paper, we analyze the stability of the Kolmogorov flow using a low-dimensional model consisting of four Fourier modes. We validate the model using numerical solutions.

Meshalkin and Sinai<sup>7</sup> provided the first solution to the stability of the Kolmogorov flow. They considered an external force per unit mass,  $\gamma \sin k_f y \hat{x}$  where  $\gamma$  is the force amplitude, and  $k_f$  is the force wavenumber. Meshalkin and Sinai<sup>7</sup> considered  $k_f = 1$ , and analyzed the stability of two-dimensional flow with  $L_x/L_y = 1/\alpha$ . They considered small perturbation

on the fundamental stream function (corresponding to the external force) and focused on its time variations. They incorporated the effects of all Fourier modes and studied the stability problem with continued fractions. An outcome of their analysis is that for  $\alpha < 1$ , the laminar solution becomes unstable at critical Reynolds number  $R_c$ ; and  $R_c \rightarrow \sqrt{2}$  (for normalization of Iudovich<sup>8</sup>) as  $\alpha \rightarrow 0$ . They observed that the laminar solution is stable for  $\alpha > 1$ . Using asymptotic instability analysis, Sivashinsky<sup>9</sup> showed that a periodically-forced two-dimensional plane-parallel flow becomes unstable beyond a critical Reynolds number. He showed the secondary flow to be chaotically self-fluctuating.

Iudovich<sup>8</sup> and Marchioro<sup>10</sup> extended the calculation of Meshalkin and Sinai<sup>7</sup> and concluded that the laminar flow is globally stable for  $\alpha \geq 1$ . For  $\alpha < 1$ , Iudovich<sup>8</sup> proved that  $R_c \rightarrow \sqrt{2}$  for  $\alpha \rightarrow 0$ , and  $R_c \rightarrow \infty$  when  $\alpha \rightarrow 1$ . They showed that  $R_c$  increases monotonically with  $\alpha$  between  $R_c = \sqrt{2}$  for  $\alpha \rightarrow 0$  and  $R_c = \infty$  for  $\alpha \rightarrow 1$ . The  $R_c$  curve represents neutral stability.

Okamoto and Shōji<sup>11</sup> performed a bifurcation analysis of the Kolmogorov flow with a finite set of Fourier modes and showed supercritical pitchfork to be the primary bifurcation. They considered 544 modes for  $\alpha > 0.3$ , even more modes for  $\alpha < 0.3$ , and observed that  $R_c = 3.011193$  for  $\alpha = 0.7$ . Using more sophisticated calculation, Nagatou<sup>12</sup> reported  $R_c$  to be bracketed between 3.011528364444 and 3.011528364446. Later, Okamoto<sup>13,14</sup> extended the bifurcation diagram to larger  $R$  using path-continuation method. Matsuda and Miyatake<sup>15</sup> studied the bifurcation diagram further and derived an exact formula for the second derivatives of their components at the bifurcation points.

The Kolmogorov flow has been simulated in experiments by inducing vortices in magnetofluids using periodically placed electrodes. Tabeling, Perrin, and Fauve<sup>16</sup> observed supercritical pitchfork bifurcation at the instability of the vortices. Bondarenko, Gak, and Dolzhanskii<sup>5</sup> performed a similar experiment. In another experiment, Sommeria<sup>17</sup> reported the existence of an inverse cascade due to the nonlinear interactions. Herault, Pétrélis, and Fauve<sup>18</sup> observed  $1/f$  noise in the nonlinear regime of the Kolmogorov flow. Tabeling<sup>19</sup> reviewed the experiments related to the Kolmogorov flow.

<sup>a)</sup>Electronic mail: soumyade@iitk.ac.in

<sup>b)</sup>Electronic mail: mkv@iitk.ac.in

Gotoh and Yamada<sup>20</sup> performed instability analysis of the rhombic cells with the stream function as  $\cos kx + \cos y$ , where  $k$  is the aspect ratio of the cell. Kim and Okamoto<sup>21</sup> performed bifurcation and inviscid limit analysis for the aforementioned rhombic cells. Thess<sup>22</sup> studied the effects of viscosity, linear friction and confinement on the flow. Platt, Sirovich, and Fitzmaurice<sup>23</sup> analyzed the Kolmogorov flow for  $k_f = 4$  and observed a sequence of bifurcations leading to chaos. For the same  $k_f$ , Chen and Price<sup>24</sup> studied the chaotic behavior using a truncation model with nine modes. In addition, researchers have studied variations of the Kolmogorov flow to three-dimensional flows<sup>25</sup>.

The Kolmogorov flow is useful not only for analyzing transition to turbulence but also for studying the inverse cascade in two-dimensional turbulence<sup>26–28</sup>. Green<sup>26</sup> reported that for  $k > k_f$ , kinetic energy spectrum,  $E(k) \sim k^{-5}$  whereas for  $k < k_f$ ,  $E(k) \sim k$ . Sommeria<sup>17</sup> studied the inverse cascade experimentally and reported that the exponent to be in the range of  $-4.5$  to  $-4.9$  for  $k > k_f$ . For  $k < k_f$ , direct numerical simulations (DNS) reveal that  $E(k) \sim k^{-5/3}$ . For random forcing in a wavenumber band near  $k = k_f$ , Gupta *et al.*<sup>27</sup> showed that for  $k > k_f$ , the energy spectrum is of the form  $k^{-3} \exp(-k^2)$ ; the exponential part gives an appearance of steeper spectrum compared to  $k^{-3}$ . Zhang *et al.*<sup>28</sup> performed a molecular simulation using Fokker-Planck method and reported that  $E(k) \sim k^{-4}$  for  $k < k_f$  due to condensation in the large scale structures. For  $k > k_f$ , Zhang *et al.*<sup>28</sup> reported that  $E(k) \sim \exp(-0.2k)$ . Energy condensate is observed at the large-scale due to inverse cascade. Gallet and Young<sup>29</sup> derived a mathematical model of energy condensation in the absence of large-scale dissipation. Mishra *et al.*<sup>30</sup> studied the condensate regime using Ekman friction. There are more works on the Kolmogorov flow, including those by Chandler and Kerswell<sup>31</sup>, Lucas and Kerswell<sup>32</sup> & Fylladitakis<sup>33</sup>, and references therein.

In this paper, we consider incompressible Kolmogorov flow in a two-dimensional periodic box with aspect ratio  $\alpha$ , and construct a low-dimensional model with four modes. We perform bifurcation analysis of the system and derive the critical Reynolds number for the instability. Our results are consistent with previous ones. Besides, we also carry out direct numerical simulations of the Kolmogorov flow for the parameter used for our model. The results from these simulations are in good agreement with those from the low-dimensional model. These results provide us confidence that the chosen modes are a good choice for the Kolmogorov flow.

The outline of this paper is as follows. In Sec. II, we present the governing equations and low-dimensional model. In Sec. III, we perform linear stability and bifurcation analysis of the low-dimensional model. We describe the energy transfers among the participating modes in Sec. IV. In Sec. V we present numerical validation using direct numerical simulation. We conclude in Sec. VI.

## II. BASIC FORMULATION -

For an incompressible flow, the Navier-Stokes equation and incompressibility condition<sup>34,35</sup> are

$$\frac{\partial \mathbf{u}}{\partial t} + \mathbf{u} \cdot \nabla \mathbf{u} = -\nabla p + \mathbf{F}_u + \nu \nabla^2 \mathbf{u}, \quad (1)$$

$$\nabla \cdot \mathbf{u} = 0, \quad (2)$$

where  $\mathbf{u}$  and  $p$  are the velocity and pressure fields respectively,  $\nu$  is the kinematic viscosity, and  $\mathbf{F}_u$  is the acceleration due to the external force. We consider two-dimensional Kolmogorov flow in a doubly-periodic box of size  $L_x \times L_y$ . The ratio  $\alpha = L_y/L_x$  is called aspect ratio. We assume density  $\rho$  to be unity. We take

$$\mathbf{F}_u = \gamma \sin\left(\frac{2\pi y k_f}{L_y}\right) \hat{x}, \quad (3)$$

where  $\gamma$  is the amplitude of the acceleration, and  $k_f$  is the forcing wavenumber which we consider to be 1.

We nondimensionalize Eqs. (1, 2) using  $L_y/2\pi$  as the length scale and  $2\pi\nu/\gamma L_y$  as the time scale, and obtain the following equations:

$$\frac{\partial \mathbf{u}}{\partial t} + \mathbf{u} \cdot \nabla \mathbf{u} = -\nabla p + \frac{1}{R} \sin(y) \hat{x} + \frac{1}{R} \nabla^2 \mathbf{u}, \quad (4)$$

$$\nabla \cdot \mathbf{u} = 0, \quad (5)$$

where

$$R = \frac{\gamma}{\nu^2} \left(\frac{L_y}{2\pi}\right)^3, \quad (6)$$

is the Reynolds number. A trivial stationary solution of the Eqs. (4, 5) is

$$\mathbf{u} = (\sin(y), 0), \quad p = \text{const.} \quad (7)$$

This solution represents a laminar flow.

For stability analysis, it is customary to work in Fourier space. In this space, the equations get transformed to

$$\frac{d}{dt} \mathbf{u}(\mathbf{k}) + \mathbf{N}_u(\mathbf{k}) = -i\mathbf{k}p(\mathbf{k}) + \mathbf{F}_u(\mathbf{k}) - \frac{1}{R} k^2 \mathbf{u}(\mathbf{k}), \quad (8)$$

$$\mathbf{k} \cdot \mathbf{u}(\mathbf{k}) = 0, \quad (9)$$

where

$$\mathbf{N}_u(\mathbf{k}) = i \sum_{\mathbf{p}} \{\mathbf{k} \cdot \mathbf{u}(-\mathbf{q})\} \mathbf{u}(-\mathbf{p}), \quad (10)$$

$$p(\mathbf{k}) = \frac{i}{k^2} \mathbf{k} \cdot [\mathbf{N}_u(\mathbf{k}) - \mathbf{F}_u(\mathbf{k})], \quad (11)$$

are the Fourier transforms of the nonlinear and pressure terms respectively. Here  $\mathbf{k} = -\mathbf{p} - \mathbf{q}$ . Note that calculation of  $\mathbf{N}_u(\mathbf{k})$  requires all possible wavenumber triads. We denote the Fourier mode as  $\mathbf{k} = (\alpha l, m)$ , where  $l, m$  are integers.

The Fourier transform of the external force  $\frac{1}{R} \sin(y) \hat{x}$  is

$$\mathbf{F}_u(\mathbf{k}) = \frac{1}{2iR} [\delta_{k_y, 1} - \delta_{k_y, -1}] \hat{x}. \quad (12)$$

That is, the forcing wavenumbers are  $(0, 1)$  and  $(0, -1)$ . Near the onset of instability, the nonlinear term  $\mathbf{u} \cdot \nabla \mathbf{u}$  generates other Fourier modes. In this paper we show that a low-dimensional model having nonzero Fourier modes at wavenumbers  $\{\mathbf{k} = (-\alpha, 0), \mathbf{p} = (0, 1), \mathbf{q} = (\alpha, -1), \text{ and } \mathbf{s} = (\alpha, 1)\}$  reproduces earlier results on Kolmogorov flow quite well (e.g. Iudovich<sup>8</sup>). In Sec. V we perform direct numerical numerical simulations and show that our low-dimensional model reproduces the simulation results to a significant degree. Due to these reasons, we work with this set of Fourier modes. We consider the following interacting triads:

$$\mathbf{k} \oplus \mathbf{p} \oplus \mathbf{q} = (-\alpha, 0) \oplus (0, 1) \oplus (\alpha, -1) = 0, \quad (13)$$

$$(-\mathbf{k}) \oplus \mathbf{p} \oplus (-\mathbf{s}) = (\alpha, 0) \oplus (0, 1) \oplus (-\alpha, -1) = 0, \quad (14)$$

where  $\oplus$  represents nonlinear interaction (see Fig. 1). Thus

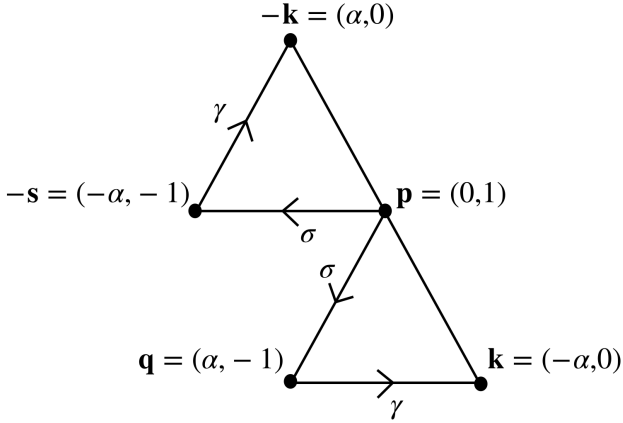


FIG. 1. Schematic representation of the triad interactions in Eqs. (13,14). Energy transfers  $\sigma$  and  $\gamma$  are  $(r-1)/(4\sqrt{2}Rr^2)$ ,  $(\alpha^2(r-1))/(4\sqrt{2}Rr^2)$ , where  $r = R/R_c$ .

possible nonlinear interactions for the modes with wavenumbers  $\mathbf{k}$ ,  $\mathbf{p}$ ,  $\mathbf{q}$  and  $\mathbf{s}$  are

$$\mathbf{k} = [(-\alpha, -1) \oplus (0, 1)] + [(-\alpha, 1) \oplus (0, -1)], \quad (15)$$

$$\mathbf{p} = [(-\alpha, 0) \oplus (\alpha, 1)] + [(\alpha, 0) \oplus (-\alpha, 1)], \quad (16)$$

$$\mathbf{q} = [(\alpha, 0) \oplus (0, -1)], \quad (17)$$

$$\mathbf{s} = [(\alpha, 0) \oplus (0, 1)]. \quad (18)$$

In the next section we derive the governing equations for the above Fourier modes.

### III. LINEAR STABILITY AND BIFURCATION ANALYSIS

The derivation of the evolution equations for the Fourier modes get simplified in Craya-Herring basis<sup>35-39</sup>. For

wavenumber  $\mathbf{k}$ , the unit vectors in this basis are<sup>35-39</sup>

$$\hat{e}_3(\mathbf{k}) = \hat{k}, \quad (19)$$

$$\hat{e}_1(\mathbf{k}) = \frac{\hat{k} \times \hat{n}}{|\hat{k} \times \hat{n}|}, \quad (20)$$

$$\hat{e}_2(\mathbf{k}) = \hat{e}_3(\mathbf{k}) \times \hat{e}_1(\mathbf{k}), \quad (21)$$

where  $\hat{k}$  is the unit vector along  $\mathbf{k}$ , and  $\hat{n} = \hat{z}$ . For all the wavenumbers under consideration,  $\hat{e}_1$  lie on the plane, while  $\hat{e}_2$  are perpendicular to the plane. Hence, for the present 2D flow,  $u_2 = 0$  for all the modes. In addition,  $u_3 = 0$  due to incompressibility condition (Eq. (9)). Therefore,

$$\mathbf{u}(\mathbf{k}) = u_1(\mathbf{k})\hat{e}_1(\mathbf{k}). \quad (22)$$

Explicitly, the unit vectors  $\hat{e}_1$ 's for the four wavenumbers  $(\mathbf{k}, \mathbf{p}, \mathbf{q}, \mathbf{s})$  are

$$\hat{e}_1(\mathbf{k}) = \hat{y}, \quad (23)$$

$$\hat{e}_1(\mathbf{p}) = \hat{x}, \quad (24)$$

$$\hat{e}_1(\mathbf{q}) = -\frac{1}{\sqrt{\alpha^2+1}}\hat{x} - \frac{\alpha}{\sqrt{\alpha^2+1}}\hat{y}, \quad (25)$$

$$\hat{e}_1(\mathbf{s}) = \frac{1}{\sqrt{\alpha^2+1}}\hat{x} - \frac{\alpha}{\sqrt{\alpha^2+1}}\hat{y}. \quad (26)$$

Using Eqs. (23-26), we derive the evolution equations for  $u_1$ 's as

$$\begin{aligned} \frac{d}{dt}u_1(\mathbf{k}) = & -\left(\frac{\alpha^2}{\sqrt{1+\alpha^2}}i\right)(u_1^*(\mathbf{p})u_1^*(\mathbf{q}) + u_1^*(\mathbf{s})u_1(\mathbf{p})) \\ & -\left(\frac{\alpha^2}{R}\right)u_1(\mathbf{k}), \end{aligned} \quad (27)$$

$$\begin{aligned} \frac{d}{dt}u_1(\mathbf{p}) = & \left(\frac{1}{\sqrt{1+\alpha^2}}i\right)(u_1^*(\mathbf{k})u_1^*(\mathbf{q}) - u_1(\mathbf{k})u_1(\mathbf{s})) \\ & + \frac{1}{2iR} - \left(\frac{1}{R}\right)u_1(\mathbf{p}), \end{aligned} \quad (28)$$

$$\frac{d}{dt}u_1(\mathbf{q}) = -\left(\frac{1-\alpha^2}{\sqrt{1+\alpha^2}}i\right)u_1^*(\mathbf{k})u_1^*(\mathbf{p}) - \left(\frac{1+\alpha^2}{R}\right)u_1(\mathbf{q}), \quad (29)$$

$$\frac{d}{dt}u_1(\mathbf{s}) = -\left(\frac{1-\alpha^2}{\sqrt{1+\alpha^2}}i\right)u_1^*(\mathbf{k})u_1(\mathbf{p}) - \left(\frac{1+\alpha^2}{R}\right)u_1(\mathbf{s}). \quad (30)$$

The steady-state solutions of the above equations are

$$S_0 : \begin{cases} u_1(\mathbf{k}) = 0, \\ u_1(\mathbf{p}) = \frac{1}{2i}, \\ u_1(\mathbf{q}) = 0, \\ u_1(\mathbf{s}) = 0, \end{cases} \quad (31)$$

$$S_1 : \begin{cases} u_1(\mathbf{k}) = -\frac{1}{\sqrt{2}r}\sqrt{r-1}, \\ u_1(\mathbf{p}) = -\frac{1}{2r}i, \\ u_1(\mathbf{q}) = -\frac{\sqrt{1+\alpha^2}}{2R}\sqrt{r-1}, \\ u_1(\mathbf{s}) = \frac{\sqrt{1+\alpha^2}}{2R}\sqrt{r-1}, \end{cases} \quad (32)$$

and

$$S_2 : \begin{cases} u_1(\mathbf{k}) = \frac{1}{\sqrt{2r}}\sqrt{r-1}, \\ u_1(\mathbf{p}) = -\frac{1}{2r}i, \\ u_1(\mathbf{q}) = \frac{\sqrt{1+\alpha^2}}{2R}\sqrt{r-1}, \\ u_1(\mathbf{s}) = -\frac{\sqrt{1+\alpha^2}}{2R}\sqrt{r-1}, \end{cases} \quad (33)$$

where  $r = R/R_c$  with

$$R_c = \frac{\sqrt{2}(1+\alpha^2)}{\sqrt{1-\alpha^2}}. \quad (34)$$

The solution  $S_0$  is valid for all  $r$ , while  $S_1$  and  $S_2$  are defined only for  $r > 1$ . Also,  $u_1(\mathbf{k}), u_1(\mathbf{q}), u_1(\mathbf{s})$  modes of  $S_1$  have opposite signs compared to  $S_2$ . See Fig. 2 for an illustration of steady  $u_1(\mathbf{k})$  for  $\alpha = 0.7$ ; the figure exhibits a transition from  $S_0$  to  $S_1$  or  $S_2$  at  $r = 1$ . For  $r > 1$ , the system follows either  $S_1$  branch or  $S_2$  branch depending on the initial condition. In subsequent subsections, we show that  $S_0$  is the only stable solution for  $r < 1$ , while  $S_1$  and  $S_2$  are the stable solutions for  $r > 1$ . For  $r > 1$ , the solution  $S_0$  is unstable. Another important point to note that  $R_c, S_1, S_2$  are not defined for  $\alpha > 1$ , hence  $S_0$  is the only solution for  $\alpha > 1$ .

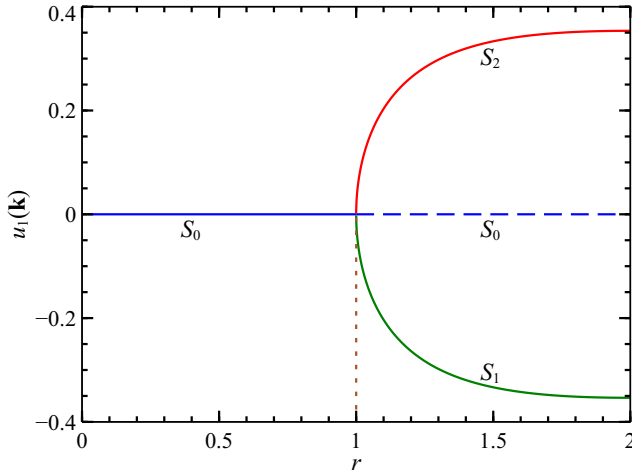


FIG. 2. (color online) For  $\alpha = 0.7$ ,  $u_1(\mathbf{k})$  as a function of  $r$ .

In the following subsections, we analyze the stability of  $S_0$ ,  $S_1$ , and  $S_2$ .

#### A. Stability of laminar solution $S_0$

First, we analyse the stability of the laminar solution,  $S_0$ . For the same, we linearize Eqs. (27-30) around  $S_0$  and obtain

the following equations:

$$\frac{d}{dt}\tilde{u}_1(\mathbf{k}) = -\left(\frac{\alpha^2}{2\sqrt{1+\alpha^2}}\right)(\tilde{u}_1^*(\mathbf{s}) - \tilde{u}_1^*(\mathbf{q})) - \left(\frac{\alpha^2}{R}\right)\tilde{u}_1(\mathbf{k}), \quad (35)$$

$$\frac{d}{dt}\tilde{u}_1(\mathbf{p}) = -\frac{1}{R}\tilde{u}_1(\mathbf{p}), \quad (36)$$

$$\frac{d}{dt}\tilde{u}_1(\mathbf{q}) = \left(\frac{1-\alpha^2}{2\sqrt{1+\alpha^2}}\right)\tilde{u}_1^*(\mathbf{k}) - \left(\frac{1+\alpha^2}{R}\right)\tilde{u}_1(\mathbf{q}), \quad (37)$$

$$\frac{d}{dt}\tilde{u}_1(\mathbf{s}) = -\left(\frac{1-\alpha^2}{2\sqrt{1+\alpha^2}}\right)\tilde{u}_1^*(\mathbf{k}) - \left(\frac{1+\alpha^2}{R}\right)\tilde{u}_1(\mathbf{s}), \quad (38)$$

where  $\tilde{u}_1(\mathbf{k}), \tilde{u}_1(\mathbf{p}), \tilde{u}_1(\mathbf{q})$  and  $\tilde{u}_1(\mathbf{s})$  represent fluctuations in  $S_0$ , and they are complex quantities. Hence we split them into real and imaginary parts:

$$\tilde{u}_1(\mathbf{k}) = \Re[\tilde{u}_1(\mathbf{k})] + i\Im[\tilde{u}_1(\mathbf{k})], \quad (39)$$

$$\tilde{u}_1(\mathbf{p}) = \Re[\tilde{u}_1(\mathbf{p})] + i\Im[\tilde{u}_1(\mathbf{p})], \quad (40)$$

$$\tilde{u}_1(\mathbf{q}) = \Re[\tilde{u}_1(\mathbf{q})] + i\Im[\tilde{u}_1(\mathbf{q})], \quad (41)$$

$$\tilde{u}_1(\mathbf{s}) = \Re[\tilde{u}_1(\mathbf{s})] + i\Im[\tilde{u}_1(\mathbf{s})]. \quad (42)$$

Using Eqs. (35-38) we derive the following matrix equation:

$$\frac{d}{dt}\mathbb{U} = \mathbb{A}\mathbb{U}, \quad (43)$$

where

$$\mathbb{A} = \begin{pmatrix} -\frac{A}{R} & 0 & 0 & 0 & B & 0 & -B & 0 \\ 0 & -\frac{A}{R} & 0 & 0 & 0 & -B & 0 & B \\ 0 & 0 & -\frac{1}{R} & 0 & 0 & 0 & 0 & 0 \\ 0 & 0 & 0 & -\frac{1}{R} & 0 & 0 & 0 & 0 \\ D & 0 & 0 & 0 & -\frac{C}{R} & 0 & 0 & 0 \\ 0 & -D & 0 & 0 & 0 & -\frac{C}{R} & 0 & 0 \\ -D & 0 & 0 & 0 & 0 & 0 & -\frac{C}{R} & 0 \\ 0 & D & 0 & 0 & 0 & 0 & 0 & -\frac{C}{R} \end{pmatrix}, \quad (44)$$

$$\mathbb{U} = \begin{pmatrix} \Re[\tilde{u}_1(\mathbf{k})] \\ \Im[\tilde{u}_1(\mathbf{k})] \\ \Re[\tilde{u}_1(\mathbf{p})] \\ \Im[\tilde{u}_1(\mathbf{p})] \\ \Re[\tilde{u}_1(\mathbf{q})] \\ \Im[\tilde{u}_1(\mathbf{q})] \\ \Re[\tilde{u}_1(\mathbf{s})] \\ \Im[\tilde{u}_1(\mathbf{s})] \end{pmatrix}.$$

Here,  $\mathbb{A}$  is a  $8 \times 8$  matrix with  $A = \alpha^2$ ,  $B = \alpha^2/(2\sqrt{1+\alpha^2})$ ,  $C = 1 + \alpha^2$  and  $D = (1 - \alpha^2)/(2\sqrt{1+\alpha^2})$ . The solution  $\mathbb{U}(t)$  is a linear combination of  $e^{\lambda t}$ , where  $\lambda$ 's are the eigenvalues of  $\mathbb{A}$ :

$$\lambda_1 = -\frac{1}{R}, \quad (45)$$

$$\lambda_2 = -\frac{C}{R}, \quad (46)$$

$$\lambda_3 = -\frac{A+C+\sqrt{(A-C)^2+8BDR^2}}{2R}, \quad (47)$$

$$\lambda_4 = -\frac{A+C-\sqrt{(A-C)^2+8BDR^2}}{2R}. \quad (48)$$

It is easy to show that  $\lambda_1, \lambda_2,$  and  $\lambda_3$  are negative for all  $\alpha$  and  $R$ . However,  $\lambda_4$  changes sign from negative to positive at the following condition, called *neutral stability condition*<sup>40</sup>:

$$\sqrt{(A-C)^2 + 8BDR^2} = A+C, \quad \text{or } R = R_c, \quad (49)$$

where  $R_c$  is given by Eq. (34).

In Fig. 3 we exhibit the  $(R, \alpha)$  phase diagram, the  $R_c$  curve, as well as the regions of stability and instability. As shown in the figure,  $R_c$  increases monotonically with  $\alpha$ , and  $R_c \rightarrow \infty$  as  $\alpha \rightarrow 1$ . Also  $R_c \rightarrow \sqrt{2}$  as  $\alpha \rightarrow 0$ . The figure shows that the system is stable below the  $R = R_c$  curve and yields the laminar solution ( $S_0$ ), and unstable otherwise. Note that for  $\alpha > 1$ , the laminar solution is stable for all  $R$ .

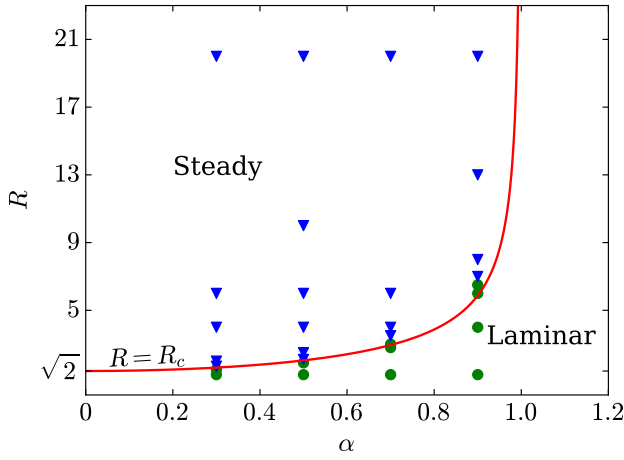


FIG. 3. (color online) Phase diagram  $(R, \alpha)$  constructed using  $R = R_c$  curve, also called neutral stability curve (the red curve). The figure also includes the steady-state results of the DNS. The green circles represent laminar solution ( $S_0$ ), but the blue triangles represent the steady vortex flow ( $S_1$  or  $S_2$ ).

In the next section we show that for  $\alpha < 1$  and  $R > R_c$ , the solutions  $S_1$  and  $S_2$  are the stable solutions.

### B. Stability analysis of $S_1$ and $S_2$

As described in Sec. III, the solutions  $S_1, S_2$  exist only for  $r > 1$ . In this subsection we show that these are stable solutions for  $r > 1$ . For the stability analysis, we generate the stability matrix for  $S_1$  and  $S_2$  by linearizing Eqs. (27-30) around  $S_1, S_2$ . This exercise yields a set of equations for  $\tilde{u}_1(\mathbf{k}), \tilde{u}_1(\mathbf{p}), \tilde{u}_1(\mathbf{q}),$  and  $\tilde{u}_1(\mathbf{s})$  similar to Eqs. (35-38). Note that  $\tilde{u}_1(\mathbf{k}), \tilde{u}_1(\mathbf{p}), \tilde{u}_1(\mathbf{q}),$  and  $\tilde{u}_1(\mathbf{s})$  are fluctuations around  $S_1, S_2$ . The resulting matrix equation is

$$\frac{d}{dt}\mathbb{U} = \mathbb{B}\mathbb{U}, \quad (50)$$

where

$$\mathbb{B} = \begin{pmatrix} -\frac{A}{R} & 0 & 0 & \pm C' & D' & 0 & -D' & 0 \\ 0 & -\frac{A}{R} & 0 & 0 & 0 & -D' & 0 & D' \\ 0 & 0 & -\frac{1}{R} & 0 & 0 & \pm E' & 0 & \pm E' \\ \mp H' & 0 & 0 & -\frac{1}{R} & \pm E' & 0 & \mp E' & 0 \\ F' & 0 & 0 & \pm G' & -\frac{C}{R} & 0 & 0 & 0 \\ 0 & -F' & \pm G' & 0 & 0 & -\frac{C}{R} & 0 & 0 \\ -F' & 0 & 0 & \mp G' & 0 & 0 & -\frac{C}{R} & 0 \\ 0 & F' & \pm G' & 0 & 0 & 0 & 0 & -\frac{C}{R} \end{pmatrix}, \quad (51)$$

and  $C', D', E', F', G'$  and  $H'$  are  $(AA')/R, (BR_c)/R, -(BA'R_c)/(AR), (DR_c)/2R, (DA'R_c)/2R$  and  $A'/R$  respectively. Here,  $A' = \sqrt{(R/R_c) - 1}$ , and  $A, B, C, D$  are same as those defined in Sec. III A.

Similar to the stability analysis for  $S_0$ , we compute the eigenvalues of the matrix  $\mathbb{B}$ , which are

$$\lambda_1 = -\frac{C}{R}, \quad (52)$$

$$\lambda_2 = -\frac{1+C+\sqrt{A+8E'G'R^2}}{2R}, \quad (53)$$

$$\lambda_3 = -\frac{1+C-\sqrt{A+8E'G'R^2}}{2R}, \quad (54)$$

$$\lambda_4 = -\frac{A+C+\sqrt{1+8D'F'R^2}}{2R}, \quad (55)$$

$$\lambda_5 = -\frac{A+C-\sqrt{1+8D'F'R^2}}{2R}, \quad (56)$$

$$\lambda_6 = -\frac{2C}{3R} + \frac{2^{\frac{4}{3}}I'R}{6O} + \frac{2^{\frac{2}{3}}O}{6R^3}, \quad (57)$$

$$\lambda_7 = -\frac{2C}{3R} - \frac{2^{\frac{4}{3}}I'R(1+\sqrt{3}i)}{12O} - \frac{2^{\frac{2}{3}}O(1-\sqrt{3}i)}{12R^3}, \quad (58)$$

$$\lambda_8 = -\frac{2C}{3R} - \frac{2^{\frac{4}{3}}I'R(1-\sqrt{3}i)}{12O} - \frac{2^{\frac{2}{3}}O(1+\sqrt{3}i)}{12R^3}. \quad (59)$$

In the above expressions,  $I'$  and  $O$  are complicated functions of  $\alpha$  and  $R$ , hence they are not presented here. The eigenvalues  $\lambda_1, \lambda_2, \lambda_3, \lambda_4, \lambda_5$  are always real and negative. However,  $\lambda_6, \lambda_7, \lambda_8$  could become complex, still their real parts are always negative. Thus, we demonstrate that the solutions  $S_1, S_2$  are stable for  $r > 1$  for which these solutions are defined. Using these observations, we also conclude that the transition at  $r = 1$  (or  $R = R_c$ ) follows a supercritical pitchfork bifurcation, as illustrated in Fig. 2 for  $\alpha = 0.7$ .

In Fig. 4 we illustrate the flow profile of the vortex pattern generated by the modes of  $S_1$  for  $\alpha = 0.7$  and  $R = 4.61$ . Note that the large scale vortical flow results from the presence of all the four modes of the model. Interestingly, the vortical flow pattern is very similar to those presented in earlier works, e.g. Okamoto and Shoji<sup>11</sup>. Note that  $R_c = 2.95$  for  $\alpha = 0.7$ .

The bifurcation mentioned above indicates that for  $\alpha < 1$ , Fourier modes with large wavenumbers get excited. In the next

section, we will describe energy transfers among the interacting Fourier modes.

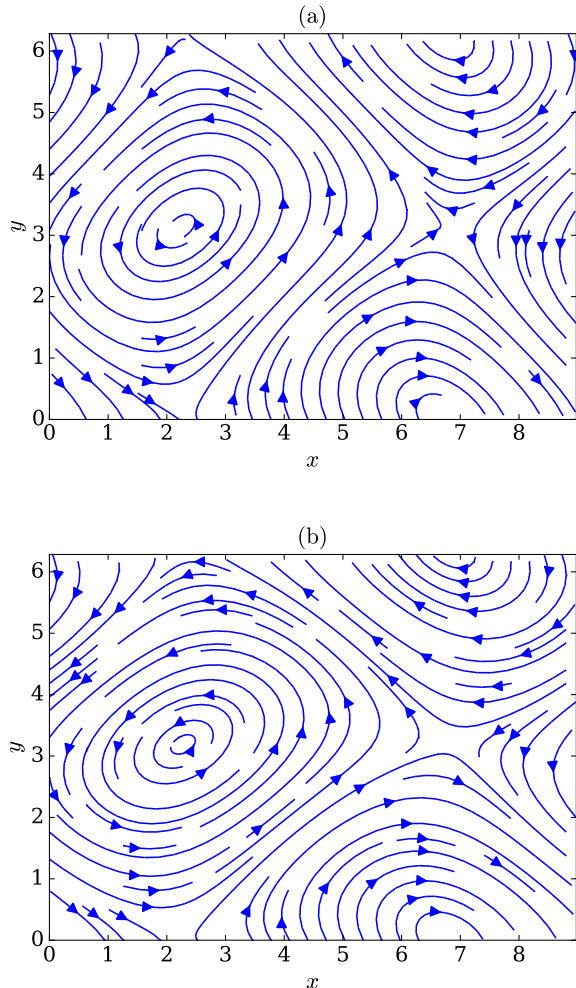


FIG. 4. (color online) (a) The flow patterns for the model solution  $S_1$  with  $\alpha = 0.7$  and  $R = 4.61$ . Here,  $L_x = 2\pi/\alpha$  and  $L_y = 2\pi$ . (b) The same steady flow pattern, is observed in DNS for the same parameters.

#### IV. ENERGY TRANSFERS IN THE KOLMOGOROV FLOW

In this section we will quantify the energy transfers between the interacting Fourier modes  $\mathbf{u}(\mathbf{k})$ ,  $\mathbf{u}(\mathbf{p})$ ,  $\mathbf{u}(\mathbf{q})$  and  $\mathbf{u}(\mathbf{s})$ . For the same we will employ the mode-to-mode energy transfer formalism proposed by Dar, Verma, and Eswaran<sup>41</sup> and Verma<sup>42</sup>. For triad  $(\mathbf{k}, \mathbf{p}, \mathbf{q})$  satisfying  $\mathbf{k} + \mathbf{p} + \mathbf{q} = 0$ , the energy transfer from  $\mathbf{u}(\mathbf{p})$  to  $\mathbf{u}(\mathbf{k})$  with the mediation of  $\mathbf{u}(\mathbf{q})$  is

$$S^{uu}(\mathbf{k}|\mathbf{p}|\mathbf{q}) = -\Im[\{\mathbf{k} \cdot \mathbf{u}(\mathbf{q})\}\{\mathbf{u}(\mathbf{p}) \cdot \mathbf{u}(\mathbf{k})\}]. \quad (60)$$

For the transfers between other Fourier modes, we employ the corresponding giver, receiver and mediator Fourier modes.

For the laminar solution  $S_0$ , energy transfers among the Fourier modes vanish due to a lack of nonzero interacting

triad. For  $S_1, S_2$ , there is no energy exchange between the Fourier modes  $\mathbf{u}(\mathbf{k})$  and  $\mathbf{u}(\mathbf{p})$ , that is,

$$S^{uu}(\mathbf{k}|\mathbf{p}|\mathbf{q}) = 0. \quad (61)$$

However, there are energy transfers among other Fourier modes. They are,

$$S^{uu}(\mathbf{k}|\mathbf{q}|\mathbf{p}) = S^{uu}(-\mathbf{k}|\mathbf{s}|\mathbf{p}) = \gamma = \frac{\alpha^2(r-1)}{4\sqrt{2}Rr^2}, \quad (62)$$

$$S^{uu}(\mathbf{q}|\mathbf{p}|\mathbf{k}) = S^{uu}(-\mathbf{s}|\mathbf{p}|\mathbf{k}) = \sigma = \frac{(r-1)}{4\sqrt{2}Rr^2}. \quad (63)$$

It is evident that  $\gamma$  and  $\sigma$  are positive because  $r > 1$ . Also  $\sigma > \gamma$  because  $\alpha < 1$ . These energy transfers are illustrated in Fig. 1.

The energy transfer computations indicate that the velocity mode  $\mathbf{u}(0, 1)$  gives energy to  $\mathbf{u}(\alpha, -1)$ , which in turn gives energy to  $\mathbf{u}(\alpha, 0)$ . Since  $\alpha < 1$ , the wavenumber  $(\alpha, 0)$  yields the largest wavelength. Thus, the energy flows from intermediate scale (corresponding to wavenumber  $(0, 1)$ ) to large scale (corresponding to wavenumber  $(\alpha, 0)$ ). Hence, we conclude that the Kolmogorov flow exhibits inverse energy cascade, contrary to the forward energy transfer observed in three-dimensional hydrodynamic turbulence.

In the next section we will describe results from direct numerical simulation and compare them with the results of the low-dimensional model.

#### V. COMPARISON WITH DIRECT NUMERICAL SIMULATIONS

In this section we will compare the results of direct numerical simulation (DNS) of the Kolmogorov flow with the model results. We numerically solve Eqs. (4, 5) using pseudospectral method in the domain  $[0, 2\pi/\alpha] \times [0, 2\pi]$  with periodic boundary conditions on all sides. We discretize the domain into  $64^2$  uniform grid points. We start the simulation with initial condition,  $\{u_1(\mathbf{k}), u_1(\mathbf{p}), u_1(\mathbf{q}), u_1(\mathbf{s})\} = \{-0.01, 0.01, -0.01(\sqrt{1+\alpha^2}/\alpha), 0.01(\sqrt{1+\alpha^2}/\alpha)\}$ , with negative wavenumbers modes given by the corresponding complex conjugates. The rest of the modes are zeros. We employ RK2 (second order Runge-Kutta) scheme for time advancement with fixed time step  $dt = 0.01$ . We employ 2/3 rule for dealiasing.

We perform the 30 runs for different values of  $\{\alpha, R\}$ , which are displayed in Fig. 3 as green circles and blue triangles. We observe that all the simulations reach steady solutions, which are either laminar solution ( $S_0$ , green dots) or vortex solution ( $S_1$  or  $S_2$ , blue triangles). Note that the two sets of simulations are nearly separated by the  $R = R_c$  curve, which is the red curve in Fig. 3. These observations indicate that our low-dimensional model captures the DNS results very well for the parameters of Fig. 3.

The dominant Fourier modes of the DNS are the same as those of the low-dimensional model. The other modes have much small magnitudes. The flow profiles of the DNS and

TABLE I. For  $\alpha = 0.7$  and  $R = 4.61$ , the relative amplitudes of the modes of low-dimensional model (LDM), as well as the relative amplitudes of the dominant modes of DNS. The total energy of the DNS is 0.188, and that for LDM is 0.18. The amplitudes are for the steady state at  $t = 440$ . The table does not include the  $-\mathbf{k}$  modes that contain the remaining 50% of the total energy.

$\mathbf{k} = (k_x, k_y)$	$E(\mathbf{k})/E(\%)$	
	(DNS)	(LDM)
$(\alpha, 0)$	16.035	15.975
$(0, 1)$	29.459	28.563
$(\alpha, 1)$	2.197	2.731
$(\alpha, -1)$	2.197	2.731
$(2\alpha, 1)$	0.053	-
$(-2\alpha, 1)$	0.053	-
$(2\alpha, 2)$	0.002	-
$(3\alpha, 1)$	0.001	-
$(\alpha, 2)$	0.001	-

the model are very similar, consistent with the above observations. For example, for the parameter values,  $\alpha = 0.7$  and  $R = 4.61$ , the steady-state flow profiles of the low-dimensional model and DNS exhibited in Figure 4 are very similar. For the same parameter values, the steady-state values of the dominant Fourier modes for the DNS and the low-dimensional model are quite close to each other (see Table I). For the DNS, the nine modes (along with their complex conjugates) listed in Table I contain nearly all of the total energy of the system.

In our DNS, we do not observe solutions other than  $S_0$ ,  $S_1$ , and  $S_2$ . That is, we do not observe any secondary bifurcation in our simulations. The DNS for  $\alpha = 0.7$  and  $R = 200$  too exhibits a steady vortical flow structure as in Fig. 4, thus indicating absence of a secondary bifurcation. Note, however, that Okamoto and Shōji<sup>11</sup> had predicted secondary bifurcations for  $\alpha = 0.98$ , as well as on the unstable branch for  $\alpha = 0.35$ . These are specialized cases that require special initial conditions and careful time-advancing of the DNS; hence, this investigation is deferred for future.

For the computation of the energy spectrum and flux, we performed a DNS for  $\alpha = 0.7$  and  $R = 200$  on a relatively higher resolution of  $512^2$ . We obtain a steady flow at  $t = 1300$ ; at this time, the energy spectrum  $E(k)$  is very steep. Steep power law of  $k^{-7}$  provides a reasonable fit to the energy spectrum, which is consistent with the predictions of Okamoto<sup>13</sup>. We also remark that the exponential function  $\exp(-2.5k)$  too provides a reasonable fit to the spectrum; this result is consistent with the arguments that the low-dimensional systems and the dissipation-range of turbulent flows exhibit exponential spectrum<sup>43,44</sup>. Note that Zhang *et al.*<sup>28</sup> obtained similar scaling in their simulation of the Kolmogorov flow. See Fig. 5(a) for an illustration.

We also compute the energy flux  $\Pi(k)$  for the same run. The energy flux is negative for the smallest wavenumber

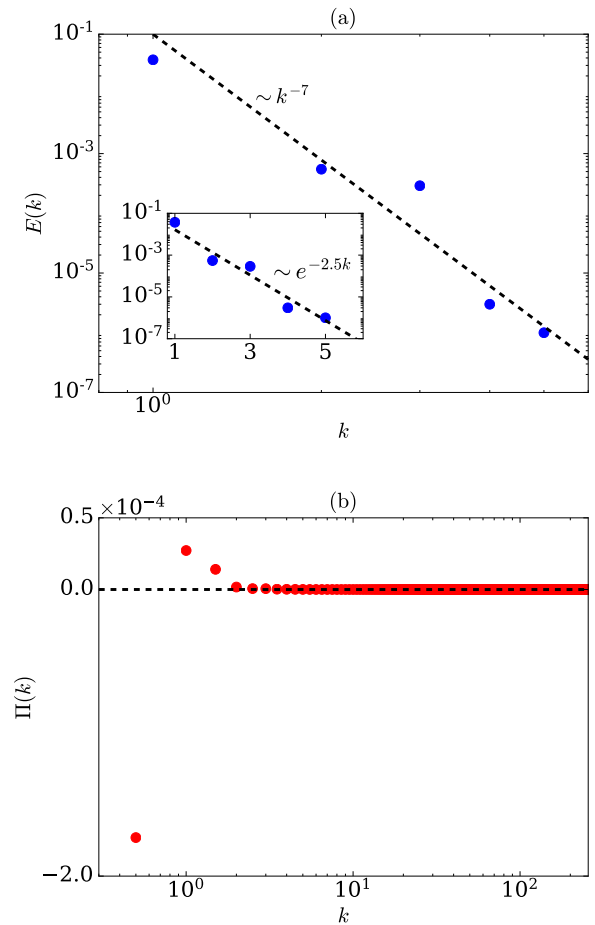


FIG. 5. (color online) For DNS with  $\alpha = 0.7$  and  $R = 200$ : (a) the energy spectrum  $E(k)$  and (b) energy flux  $\Pi(k)$ . Both power law ( $k^{-7}$ ) and exponential function ( $\exp(-2.5k)$ ) [see inset of (a)] fit with the numerical data reasonably well.  $\Pi(k)$  is negative for the lowest wavenumber, indicating inverse cascade. Also,  $\Pi(k)$  is negligible for  $k > 3$  due to the dominance of small wavenumber modes.

sphere of radius 0.5, indicating an inverse cascade of energy (see Fig. 5(b)). The simulation result is close to the model result, that is, the energy transfer from  $u_1(-\alpha, -1)$  to  $u_1(\alpha, 0)$  shown in Fig. 1 and discussed in Sec. IV. In addition,  $\Pi(k)$  falls sharply. Thus, both the energy spectrum and flux support earlier observations that only small wavenumber modes are active in the Kolmogorov flow. For example, see Table I. We conclude in the next section.

## VI. DISCUSSIONS AND CONCLUSIONS

In this paper, we present a low-dimensional model that captures the essential features of the Kolmogorov flow. The Fourier components are in the Craya-Herring basis. We identify the fixed points of the system, and show that the system bifurcates from the laminar solution to a new solution with

vortex structure. These solutions are consistent with earlier works based on analytical, numerical, and experimental tools. In addition, we perform direct numerical simulation (DNS) of the Kolmogorov flow that exhibits similar results as the low-dimensional model.

Our low-dimensional model captures the critical Reynolds number of the Kolmogorov flow. The model predicts that the new vortex solution remains stable beyond  $R > R_c$ . The critical Reynolds number  $R_c$  increases monotonically with  $\alpha$ , with  $R_c \rightarrow \sqrt{2}$  as  $\alpha \rightarrow 0$ , and  $R_c \rightarrow \infty$  as  $\alpha \rightarrow 1$ . But between these two limits, the model prediction of  $R_c$  is marginally lower than those computed using models containing a larger number of Fourier modes<sup>11,12</sup>. Using energy transfers, we show that in the Kolmogorov flow, the energy flows from intermediate scales to large scales; this is contrary to the forward energy transfers in Kolmogorov's theory of turbulence. Thus, our model captures essential aspects of the primary bifurcation of the Kolmogorov flow, and its results are consistent with earlier models.

Our DNS results are very similar to those of the low-dimensional model. For example, the flow patterns and the dominant modes of DNS are close to those of the low-dimensional model. Both DNS and the model do not exhibit any secondary bifurcation, indicating the robustness of the low-dimensional model. It is interesting to note that the six-mode dynamo model of Verma *et al.*<sup>45</sup> showed very similar bifurcation, as described in this paper. It is possible that the Kolmogorov flow with forcing at larger wavenumbers ( $k_f > 1$ ) may exhibit secondary bifurcation.

There are certain discrepancies between the predictions of our model and those of earlier models. As shown by Okamoto and Shōji<sup>11</sup>, we expect secondary bifurcations for  $\alpha$  very close to unity, as well as on the unstable branch for other  $\alpha$ 's. A verification of Okamoto and Shōji<sup>11</sup>'s predictions on secondary bifurcations using DNS requires major fine-tuning of the initial conditions and the DNS, and it is planned for the future. Also, our model does not capture several oscillatory solutions predicted by Sivashinsky<sup>9</sup>. These issues need to be explored in the future.

In summary, our four-model model captures many of its interesting features of the Kolmogorov flow. It also opens avenues for further explorations of the Kolmogorov flow with  $k_f > 1$  and large Reynolds numbers.

## VII. ACKNOWLEDGEMENTS

We thank Roshan Samuel, Shashwat Bhattacharya, Mohammad Anas, Narendra Pratap, Akanksha Gupta, Shadab Alam, and Manohar Sharma for useful discussions. This work was supported by the research grant 6104-1 from Indo-French Centre for the Promotion of Advanced Research (IFC-PAR/CEFIPRA). Soumyadeep Chatterjee is supported by INSPIRE fellowship (IF180094) of Department of Science & Technology, India.

## VIII. DATA AVAILABILITY

The data that support the findings of this study are available from the corresponding author upon reasonable request.

## IX. REFERENCES

- <sup>1</sup>V. I. Arnol'd and L. D. Meshalkin, "A. N. Kolmogorov's seminar on selected problems of analysis (1958-1959)," *Usp. Mat. Nauk* **15**, 247–250 (1960).
- <sup>2</sup>A. M. Obukhov, "Kolmogorov flow and laboratory simulation of it," *Russ. Math. Surv.* **38**, 113–126 (1983).
- <sup>3</sup>V. I. Arnol'd, "Kolmogorov's hydrodynamic attractors," *Proc.: Math. and Phsc.* **434**, 19–22 (1991).
- <sup>4</sup>J. M. Burgess, C. Bizon, W. D. McCormick, J. B. Swift, and H. L. Swinney, "Instability of the Kolmogorov flow in a soap film," *Phys. Rev. E* **60**, 715 (1999).
- <sup>5</sup>N. F. Bondarenko, M. Z. Gak, and F. V. Dolzhanskii, "Laboratory and theoretical models of plane periodic flow," *Akademiia Nauk SSSR, Izvestiia, Fizika Atmosfery i Okeana* **15**, 1017–1026 (1979).
- <sup>6</sup>B. Suri, J. Tithof, R. Mitchell, R. O. Grigoriev, and M. Schatz, "Velocity profile in a two-layer Kolmogorov like flow," *Phys. Fluids* **26**, 053601 (2014).
- <sup>7</sup>L. D. Meshalkin and Y. G. Sinai, "Investigation of the stability of a stationary solution of a system of equations for the plane movement of an incompressible viscous liquid," *J. Appl. Math. Mech.* **25**, 1700–1705 (1961).
- <sup>8</sup>V. I. Iudovich, "Example of the generation of a secondary stationary or periodic flow when there is loss of stability of the laminar flow of a viscous incompressible fluid," *J. Appl. Math. Mech.* **29**, 527–544 (1965).
- <sup>9</sup>G. I. Sivashinsky, "Weak turbulence in periodic flows," *Physica D Nonlinear Phenomena* **17**, 243–255 (1985).
- <sup>10</sup>C. Marchioro, "An example of absence of turbulence for any Reynolds number," *Commun. Math. Phys.* **108**, 647–651 (1987).
- <sup>11</sup>H. Okamoto and M. Shōji, "Bifurcation diagrams in Kolmogorov's problem of viscous incompressible fluid on 2-D flat tori," *Jpn. J. Ind. Appl. Math.* **10**, 191–218 (1993).
- <sup>12</sup>K. Nagatou, "A computer-assisted proof on the stability of the Kolmogorov flows of incompressible viscous fluid," *J. Comput. Appl. Math.* **169**, 33–44 (2004).
- <sup>13</sup>H. Okamoto, "Nearly singular two-dimensional Kolmogorov flows for large Reynolds numbers," *J. Dyn. Diff. Eqn.* **8**, 203–220 (1996).
- <sup>14</sup>H. Okamoto, "A study of bifurcation of Kolmogorov flows with an emphasis on the singular limit," *Doc. Math. J. DMV Extra Volume ICM* **3**, 513–522 (1998).
- <sup>15</sup>M. Matsuda and S. Miyatake, "Bifurcation analysis of Kolmogorov flows," *Tohoku Math. J.* **54**, 329–365 (2002).
- <sup>16</sup>P. Tabeling, B. Perrin, and S. Fauve, "Instability of a Linear Array of Forced Vortices," *EPL* **3**, 459–465 (1987).
- <sup>17</sup>J. Sommeria, "Experimental study of the two-dimensional inverse energy cascade in a square box," *J. Fluid Mech.* **170**, 139–168 (1986).
- <sup>18</sup>J. Herault, F. Pétrélis, and S. Fauve, "Experimental observation of 1/f noise in quasi-bidimensional turbulent flows," *EPL* **111**, 44002 (2015).
- <sup>19</sup>P. Tabeling, "Two-dimensional turbulence: a physicist approach," *Phys. Rep.* **362**, 1–62 (2002).
- <sup>20</sup>K. Gotoh and M. Yamada, "The instability of rhombic cell flows," *Fluid Dyn. Res.* **1**, 165–176 (1987).
- <sup>21</sup>S. C. Kim and H. Okamoto, "Bifurcations and inviscid limit of rhombic Navier-Stokes flows in tori," *IMA J. Appl. Math.* **68**, 119–134 (2003).
- <sup>22</sup>A. Thess, "Instabilities in two-dimensional spatially periodic flows. I. Kolmogorov flow," *Phys. Fluids A* **4**, 1385–1395 (1992).
- <sup>23</sup>N. Platt, L. Sirovich, and N. Fitzmaurice, "An investigation of chaotic Kolmogorov flows," *Phys. Fluids A* **3**, 681 (1991).
- <sup>24</sup>Z. M. Chen and W. G. Price, "Chaotic behavior of a Galerkin model of a two-dimensional flow," *Chaos* **14**, 1056 (2004).
- <sup>25</sup>I. E. Sarris, H. Jeanmart, D. Carati, and G. Winckelmans, "Box-size dependence and breaking of translational invariance in the velocity statistics



- computed from three-dimensional turbulent Kolmogorov flows,” *Phys. of Fluids* **19**, 095101 (2007).
- <sup>26</sup>J. S. A. Green, “Two-dimensional turbulence near the viscous limit,” *J. Fluid Mech.* **62**, 273–287 (1974).
- <sup>27</sup>A. Gupta, R. Jayaram, A. G. Chatterjee, S. Sadhukhan, R. Samtaney, and M. K. Verma, “Energy and enstrophy spectra and fluxes for the inertial-dissipation range of two-dimensional turbulence,” *Phys. Rev. E* **100**, 053101 (2019).
- <sup>28</sup>J. Zhang, P. Tian, S. Yao, and F. Fei, “Multiscale investigation of Kolmogorov flow: From microscopic molecular motions to macroscopic coherent structures,” *Phys. of Fluids* **31**, 082008 (2019).
- <sup>29</sup>B. Gallet and W. R. Young, “A two-dimensional vortex condensate at high Reynolds number,” *J. Fluid Mech.* **715**, 359–388 (2013).
- <sup>30</sup>P. K. Mishra, J. H erault, S. Fauve, and M. K. Verma, “Dynamics of reversals and condensates in two-dimensional Kolmogorov flows,” *Phys. Rev. E* **91**, 053005 (2015).
- <sup>31</sup>G. J. Chandler and R. R. Kerswell, “Invariant recurrent solutions embedded in a turbulent two-dimensional Kolmogorov flow,” *J. Fluid Mech.* **722**, 554–595 (2013).
- <sup>32</sup>D. Lucas and R. Kerswell, “Spatiotemporal dynamics in 2D Kolmogorov flow over large domains,” *J. Fluid Mech.* **750**, 518–554 (2014).
- <sup>33</sup>E. Fylladitakis, “Kolmogorov Flow: Seven Decades of History,” *J. Appl. Math. Phys.* **6**, 2227–2263 (2018).
- <sup>34</sup>M. K. Verma, *Physics of Buoyant Flows: From Instabilities to Turbulence* (World Scientific, Singapore, 2018).
- <sup>35</sup>M. K. Verma, *Energy transfers in Fluid Flows: Multiscale and Spectral Perspectives* (Cambridge University Press, Cambridge, 2019).
- <sup>36</sup>A. Craya, *Contribution   l’analyse de la turbulence associ e   des vitesses moyennes*, Ph.D. thesis, Universit  de Grenoble (1958).
- <sup>37</sup>J. R. Herring, “Approach of axisymmetric turbulence to isotropy,” *Phys. Fluids* **17**, 859–872 (1974).
- <sup>38</sup>M. Lesieur, *Turbulence in Fluids* (Springer-Verlag, Dordrecht, 2008).
- <sup>39</sup>P. Sagaut and C. Cambon, *Homogeneous Turbulence Dynamics*, 2nd ed. (Cambridge University Press, Cambridge, 2018).
- <sup>40</sup>S. Chandrasekhar, *Hydrodynamic and Hydromagnetic Stability* (Oxford University Press, Oxford, 2013).
- <sup>41</sup>G. Dar, M. K. Verma, and V. Eswaran, “Energy transfer in two-dimensional magnetohydrodynamic turbulence: formalism and numerical results,” *Physica D* **157**, 207–225 (2001).
- <sup>42</sup>M. K. Verma, “Statistical theory of magnetohydrodynamic turbulence: recent results,” *Phys. Rep.* **401**, 229–380 (2004).
- <sup>43</sup>S. Paul, P. K. Mishra, M. K. Verma, and K. Kumar, “Order and chaos in two-dimensional Rayleigh-B enard convection,” , arXiv:0904.2917 (2009).
- <sup>44</sup>A. Bershadskii, “Near-dissipation range in nonlocal turbulence,” *Phys. Fluids* **20**, 085103 (2008).
- <sup>45</sup>M. K. Verma, T. Lessinnes, D. Carati, I. E. Sarris, K. Kumar, and M. Singh, “Dynamo transition in low-dimensional models,” *Phys. Rev. E* **78**, 036409 (2008).